Journal of Sound and Vibration (2000) **230**(4), 851–875
doi:10.1006/jsvi.1999.2658, available online at http://www.idealibrary.com on IDEAL®

A METHOD FOR THE VIBRATION ANALYSIS OF BUILT-UP STRUCTURES, PART II: ANALYSIS OF THE PLATE-STIFFENED BEAM USING A COMBINATION OF FINITE ELEMENT ANALYSIS AND ANALYTICAL IMPEDANCES

R. M. GRICE AND R. J. PINNINGTON

Institute of Sound and Vibration Research, University of Southampton, Southampton, SO17 IBJ, England

(*Received* 13 *April* 1999, *and in final form* 16 *September* 1999)

This is the second of two companion papers which collectively present a method for the analysis of complex structures built-up from stiff beams and flexible plates. The method separates the stiff parts of the structure (which support the vibration sources) and the flexible parts of the structure, models the two parts separately in order to accommodate the significantly different wavelengths of the waves in them, then recombines the two parts to obtain the response of the complete structure. The companion paper analyzed the plate-stiffened beam consisting of a directly driven uniform beam attached to a rectangular plate in order to demonstrate the theoretical foundation of the method. However, the theoretical work is limited to very simple geometries. Hence, this paper implements the method using a combination of numerical analysis to model the stiff beam and analytical impedances to model the flexible plate. In particular, the response of the beam separate from the plate is modelled using finite element analysis. The response of the plate separate from the beam is modelled using analytical impedances in a manner identical to that used in the companion paper. The two separate responses are finally coupled together using a standard sub-structuring procedure. Predictions of input and transfer response for two geometrically different plate-stiffened beams, one with a rectangular plate and one with a trapezoidal plate, compare well with measurements. Additionally, the method allows estimation of the mean-square acceleration of the plates which also compare favourably with measurements

1. INTRODUCTION

The companion paper [1] showed that in the plate-stiffened beam of Figure 1, the difference in the wavelengths of the long waves in the stiff beam and the short waves in the flexible plate is quite large. In fact, it was demonstrated formally that provided the long waves have at least twice the wavelength of the short waves, the plate presents a *locally reacting impedance* to the beam. This means that the

0022-460X/00/090851 + 25 $35.00/0

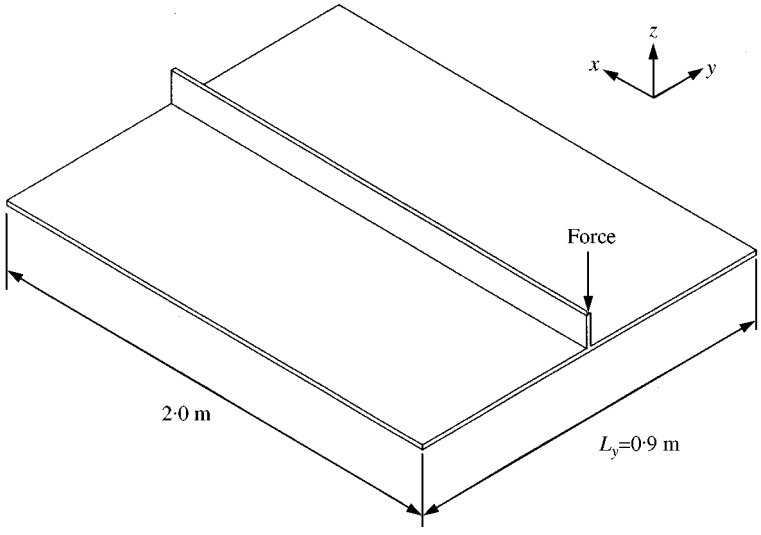

Figure 1. The experimental plate-stiffened beam. The force acts at one end of the beam as shown. The beam is 68 mm high excluding the thickness of the plate. Both beam and plate are 5·9 mm thick. The material properties are given in Table 1.

response of the plate depends almost entirely on waves which radiate into the plate normal to the axis of the beam. In practice, this means that the continuous plate shown in Figure 1 can be replaced physically with a large number of narrow parallel-sided strips of plate without significantly altering the response of the entire structure. Using this finding, a general theoretical method for the analysis of built-up structures was proposed in reference [1]. The theoretical method utilizes the large difference in the wavelengths of the long and short waves to separate the complete structure into separate *spine* and *receiver* components, the former which carries long waves and the later which carries much shorter waves. The response of the complete structure is then predicted in three steps. First, the response of the spine separate from the receiver is established; second, the locally reacting impedence of the receiver is determined; third, the separate spine and receiver responses are combined to yield the response of the complete structure.

Applying this theoretical method to the plate-stiffened beam, the dispersion relation for a wave with wavenumber k_b and frequency ω in the beam when *uncoupled* from the plate is [2]

$$\tilde{D}_b k_b^4 = m_b' \omega^2, \tag{1}$$

where $\tilde{D}_b, m_b'$ are the complex stiffness and mass per unit length respectively (Appendix A contains a list of symbols). In reference [1] it was shown that the plate in Figure 1 presents a locally reacting impedance per unit length along the beam given by

$$\tilde{Z}^{R'} = \frac{2m_p'' \omega}{k_y}\left(\frac{1-\tilde{\beta}_y}{1+\tilde{\beta}_y} + \mathrm{j}\right), \quad \tilde{\beta}_y = \mathrm{e}^{-\mathrm{j}\tilde{k}_y L_y} \tag{2}$$

where m''_p is the plate mass per unit area, k_y is the wavenumber for the waves which radiate into the plate normal to the beam axis and L_y is the width of the plate normal to the beam. Equation (2) is the impedance of a strip of plate of unit width and length L_y driven at its midpoint and is essentially a function of only two parameters, namely k_y and L_y. It was termed the *receiver impedance* in reference [1]. Finally, it was shown in reference [1] that the dispersion relation for the beam coupled to the locally reacting plate is given by

$$\tilde{D}_b k_{psb}^4 = m'_b \omega^2 - \mathrm{j}\omega \tilde{Z}^{R'}, \tag{3}$$

where k_{psb} is the wavenumber in the beam when coupled to the plate. Equation (3) is recognizable as a combination of equations (1) and (2). In reference [1], equation (3) was used to predict the input and transfer frequency response functions of two slightly different plate-stiffened beams. The predictions compared favourably with laboratory measurements, thereby supporting both the theoretical method and the underlying physical argument.

1.1. EXTENDING THE METHOD TO MORE COMPLEX BUILT-UP STRUCTURES

Despite successfully predicting the response of the plate-stiffened beam of Figure 1, the analytical approach adopted in reference [1] is limited to geometrically simple structures such as a uniform beam attached to a rectangular plate. It is impractical, for example, when applied to the structure shown in Figure 2 (in which the plate has a trapezoidal area) because the impedance of the plate varies along the beam. However, provided the receiver presents a locally reacting impedance to the spine, it can still be replaced physically by a number of narrow parallel-sided strips of plate which collectively can form any required geometry. For example, Figure 3 shows the rectangular plate-stiffened beam partitioned into two components. One component represents the beam; the other represents the rectangular plate with a number of narrow plate-strips. As in reference [1], the response of the structure is determined by applying the three steps of the theoretical method as follows. First, the response of the spine is calculated in isolation of the receiver. In principle, any method which predicts the spine response is viable. However, given that the spine carries long waves having a wavelength comparable with its overall length, a finite element model of the spine is appealing. Second, the receiver is modelled as a number of plate strips using equation (2). Third, the responses of the spine and receiver are combined to yield the response of the complete structure. Such a procedure, combining numerical (finite element) and analytical analyses, will be termed the *hybrid method* in this paper.

The companion paper formally determined the conditions which need to be fulfilled in order to apply the theoretical method, as well as identifying the parameters needed to model the receiver impedance. This paper completes the work by addressing the following objectives: (a) determination of the parameters needed to model the response of the spine; and (b) determination of the parameters required when the separate responses of the receivers and spine are combined.

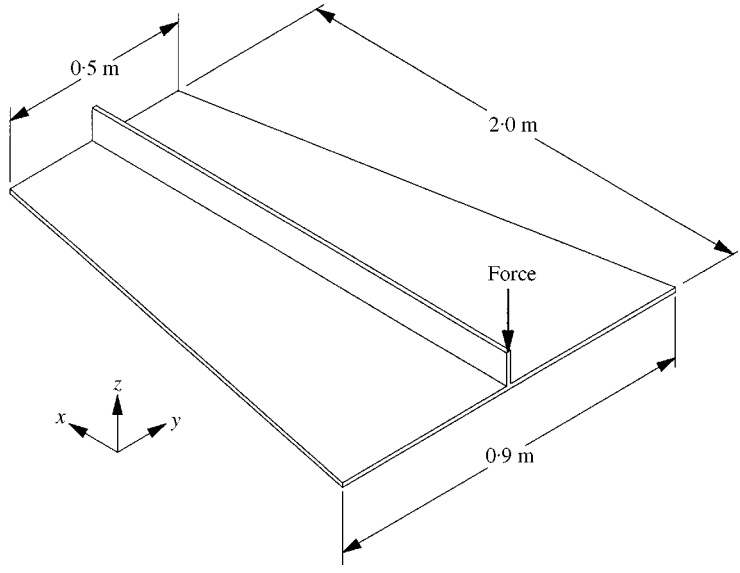

Figure 2. The trapezoidal plate-stiffened beam. The beam is 68 mm high excluding the thickness of the plate. Both beam and plate are 5·9 mm thick. The material properties are given in Table 1.

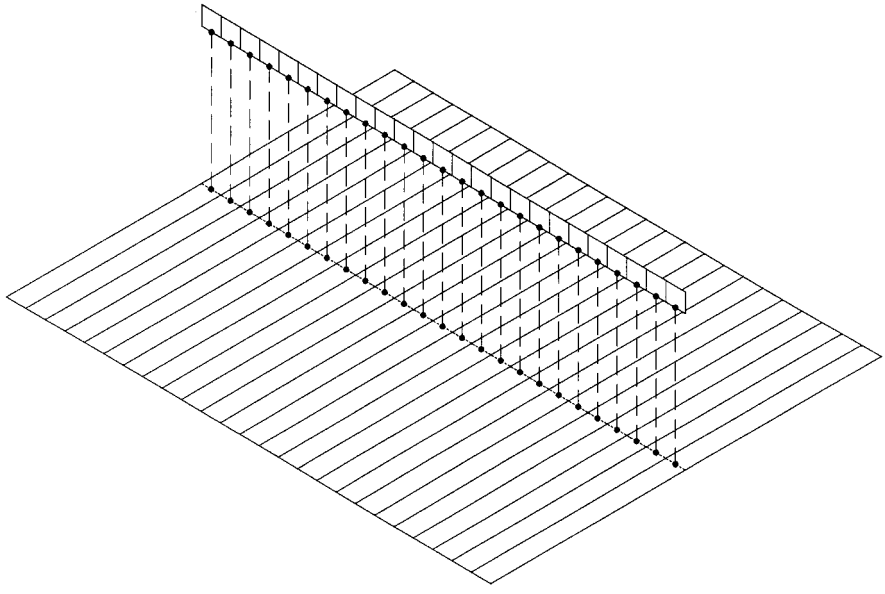

Figure 3. The plate-stiffened beam split into a beam attached to a set of independent narrow strips of plate (the receivers).

The hybrid method is applied to both the rectangular and trapezoidal plate-stiffened beams. Predictions of the input and transfer frequency response functions on the spine beam are compared with laboratory measurements. In passing, it is shown how the hybrid method facilitates straightforward prediction of

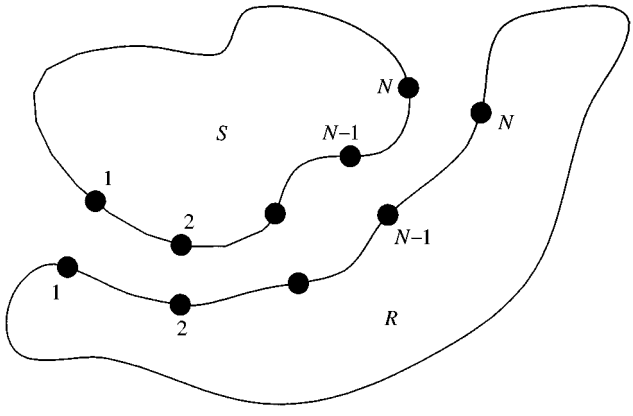

Figure 4. Two structures which are to be joined at a number of points "N".

the mean-square vibration of the plate which is compared with measurements. The mean-square response of the plate could be used to predict sound radiation.

2. THE HYBRID METHOD

The hybrid method uses a standard sub-structuring procedure (e.g. reference [3]) to couple the spine and receivers. The procedure is recapitulated below.

Figure 4 shows two continuous structural components S and R. In the present context S is the spine and R is the receiver. Both structures have, in general, an infinite number of degrees of freedom. It is required to couple the structures at a finite number of points N.

If the spine is analyzed on its own, one can compute the frequency response function between any two of the chosen degrees of freedom. By determining all the input and transfer frequency response functions between these degrees of freedom, a mobility matrix $\tilde{\mathbf{Y}}^S$ can be assembled. The process can be repeated on the receiver to produce its mobility matrix $\tilde{\mathbf{Y}}^R$.

To couple the two components, both mobility matrices are inverted to produce impedance matrice.

$$\tilde{\mathbf{Z}}^S = \tilde{\mathbf{Y}}^{S^{-1}}, \qquad \tilde{\mathbf{Z}}^R = \tilde{\mathbf{Y}}^{R^{-1}}. \tag{4}$$

Using the compatibility of the velocities at their interconnecting points, the coupled impedance matrix is simply

$$\tilde{\mathbf{Z}}^C = \tilde{\mathbf{Z}}^S + \tilde{\mathbf{Z}}^R. \tag{5}$$

The coupled mobility matrix is found after another inversion

$$\tilde{\mathbf{Y}}^C = \tilde{\mathbf{Z}}^{C^{-1}}. \tag{6}$$

In the past, the inversion of large matrices has been avoided because the amount of computation required was too expensive and the inversion could become unstable

if insufficient accuracy was available during the calculations [4]. Modern high-speed digital computers have ameliorated the first difficulty but not the second. The direct computation of a matrix inverse is usually avoided because it requires the matrix determinant. Instead, factorization algorithms which do not compute the determinant are deployed [5].

The numerical accuracy of inversion of a square matrix $\mathbf{A}$ can be estimated using the condition number

$$\text{cond}(\mathbf{A}) = \|\mathbf{A}\| \, \|\mathbf{A}^{-1}\|, \tag{7}$$

where $\| \ldots \|$ indicates the norm of the matrix. It can be shown [4] that the inversion is stable provided

$$\text{cond}(\mathbf{A}) \ll (nr)^{-1}, \tag{8}$$

where n is the precision of the floating point numbers stored by the computer and r is the unit round-off [4]. Using a 486 personal computer, the matrix inversion could be considered stable if the condition numbers remained below 10^{14}.

The condition number on its own does not guarantee accuracy. Thus, the calculations in the hybrid method which lead to the coupled mobility matrix in equation (6) included the following checks.

(i) The condition numbers for both the spine mobility matrix and the coupled impedance matrix are calculated prior to inversion and checked against equation (8).

(ii) The condition number of both matrices should fall with increasing frequency, indicating increasing numerical stability. This is because damping causes the magnitudes of the off-diagonal transfer responses to fall below those of the input responses on the leading diagonal, and this difference increases with frequency.

(iii) For a structure excited by a vector of harmonic forces $\tilde{\mathbf{F}}$ the time-averaged power $\bar{P}$ injected into it is

$$\bar{P} = \tfrac{1}{2} \text{Re}\{\tilde{\mathbf{F}}^{*\text{T}} \, \tilde{\mathbf{Y}}^{C} \, \tilde{\mathbf{F}}\}. \tag{9}$$

For a damped structure, equation (9) must be positive.

3. APPLICATION OF THE HYBRID METHOD TO THE PLATE-STIFFENED BEAM

Figure 3 represented the rectangular plate-stiffened beam as a spine attached to a number of independent plate strips (the receivers). The number and width of the receivers are parameters which will be quantified below. The following sections detail the finite element analysis of the beam, the use of the receiver impedance of equation (2), the process of coupling the two separate responses to obtain the response of the structure, and lastly the calculation of the mean-square response of the receivers.

3.1. FINITE ELEMENT ANALYSIS OF THE SPINE BEAM

The first step in the hybrid method is the calculation of the spine mobility matrix $\mathbf{Y}^S$. This involves the selection of a suitable finite element, determination of the element dimensions, definition of the points to which receivers will be attached, construction of the mesh and computation of the frequency response functions.

In Figure 1, the beam neutral axis can be expected to lie in the mid-plane of the plate because the plate is very stiff in-plane. Therefore, to accomodate this offset neutral axis, an 8-noded quadrilateral plate element was selected to model the beam. These elements would model the flexible motion via in-plane bending [6]. In general, the accuracy of finite element analysis increases as the element size decreases. Petyt [6] suggests that a *minimum* of four quadratic elements are needed per wavelength to obtain natural frequency predictions with an accuracy better than 1%. To ensure that the finite element model of the beam was at least this accurate, the element length was set at 0·08 m such that there would be at least six elements per wavelength at the maximum frequency. The elemental height was 0·0739 m which included the thickness of the plate.

Figure 5 shows the finite element model of the beam. This material properties are shown in Table 1. To simulate the experimental conditions which will be presented in section 5 more exactly, a unit harmonic force $\tilde{f}_1$ was applied at the upper edge of the beam. In order to locate the neutral axis of the beam close to that in the real structure, constraints were applied to prevent axial deformation along its lower edge. This places the neutral axis at the lower edge of the beam in Figure 1 which produces an increase in the beam stiffness compared to that used in reference [1]. Additional boundary conditions were applied to ensure that the beam could only translate and rotate in the x–y plane ($\theta_x = 0$, $\theta_y = 0$ at all nodes) to replicate the experimental conditions in reference [1]. The final mesh had 25 elements and 333 unconstrained degrees of freedom. The overall input and transfer responses of the structure were required at the ends of the beam as shown by the velocities $\tilde{v}_1$, $\tilde{v}_2$ in Figure 5.

3.2. RECEIVER IMPEDANCE

The theory in section 2 used the mobility of both the spine and the receiver components in order to calculate the coupled mobility matrix of the complete structure. However, in the present case it is not necessary to form the receiver mobility matrix and then invert it because the impedances can be found directly. Figure 3 shows a number of points "●" to which receivers are connected. With this arrangement, there are as many receivers as finite elements. The impedance of each receiver is determined by multiplying the impedance per unit width of equation (2) by the receiver width which in this case matches the element length along the beam. Thus, the receiver impedance is

$$\tilde{Z}^R = \tilde{Z}^{R'} L_e \quad \left(\frac{N}{\text{ms}}\right). \tag{10}$$

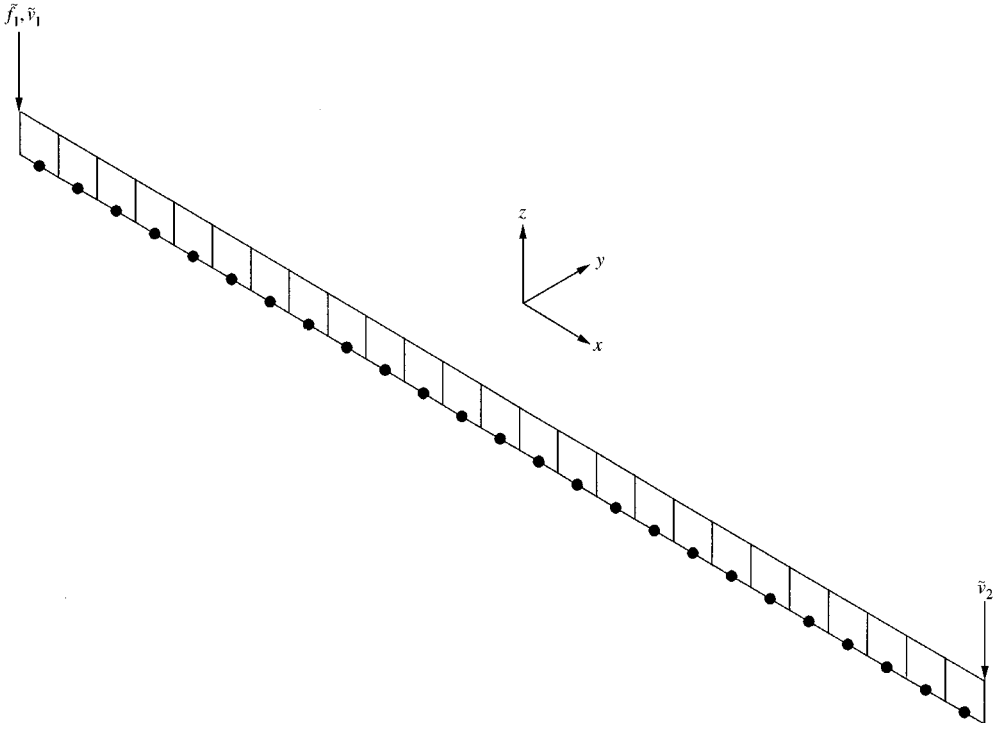

Figure 5. The finite element mesh of the beam. Each element has a length of 0·08 m in the x-direction and 0·0739 m in the y-direction. Boundary conditions: $u_x = 0$ along lower edge, $\theta_x = \theta_y = 0$ at all nodes.

TABLE 1

Material properties for the plate-stiffened beams

Young's modulus (GN/m^2)	Poisson's ratio (−)	Loss factor (−)	Density (kg/m^3)
4·4	0·38	0·05	1152

where $L_e = 0{\cdot}08$ m is the element length along the beam. The receiver length L_y in equation (2) is 0·9 m which equals the width of the plate normal to the beam. For the trapezoidal plate-stiffened beam of Figure 2, the plate can be represented approximately using receivers of varying lengths as shown in Figure 6.

3.3. CALCULATION OF THE COUPLED RESPONSE

Since there are 25 receivers to be coupled to the spine and two additional points on the ends of the spine at which velocities are to be computed, 27 frequency

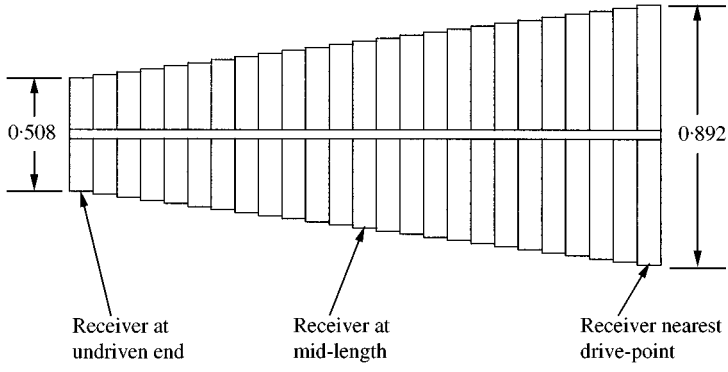

Figure 6. Plan of the trapezoidal plate-stiffened beam (structure "C") showing the idealisation of the plate as a set of varying-length receivers.

response functions (one input and 26 transfer) must be calculated for each position of the excitation force along the beam. The full spine mobility matrix is found by calculating 27 frequency response functions for each of the 27 positions along the beam.

The frequency response functions were calculated by direct solution of the equations of motion in the frequency domain rather than by modal superposition [6]. This method takes longer than model superposition but was done for simplicity. The ANSYS finite element program was used to perform the calculations [7]. However, because the mesh has so few degrees of freedom, the forced response is still quite efficient. Using 250 frequencies between 10 Hz and 1 kHz required 4·7 h computation using a 300 MHz personal computer. This resulted in $27^2 = 729$ frequency response functions.

The coupling of the finite element response of the spine to the 25 receiver impedances was carried out using MATLAB [8]. The time taken to compute the coupled response together with the associated stability calculations was only 30 s. These timings highlight that, once the relatively time-consuming finite element analysis is complete, the hybrid method allows rapid prototyping of the spine response using various plate geometries.

3.4. PREDICTION OF THE MEAN-SQUARE RESPONSE OF THE PLATE

As part of the sub-structuring procedure, the hybrid method calculates the coupled velocities at the joint between the spine and the receivers. Using the receiver impedances of equation (10), the power input to the receivers can be determined. This can be used to estimate the mean-square response of the receivers.

For each receiver, the time-averaged power $\bar{P}_R$ injected into it by the spine beam vibrating with velocity $\tilde{v}_S$ is calculated using [2]

$$\bar{P}_R = \tfrac{1}{2}|\tilde{v}_S|^2 \ \mathrm{Re}\{\tilde{Z}^R\} = \eta_R \omega \bar{E}_R, \tag{11}$$

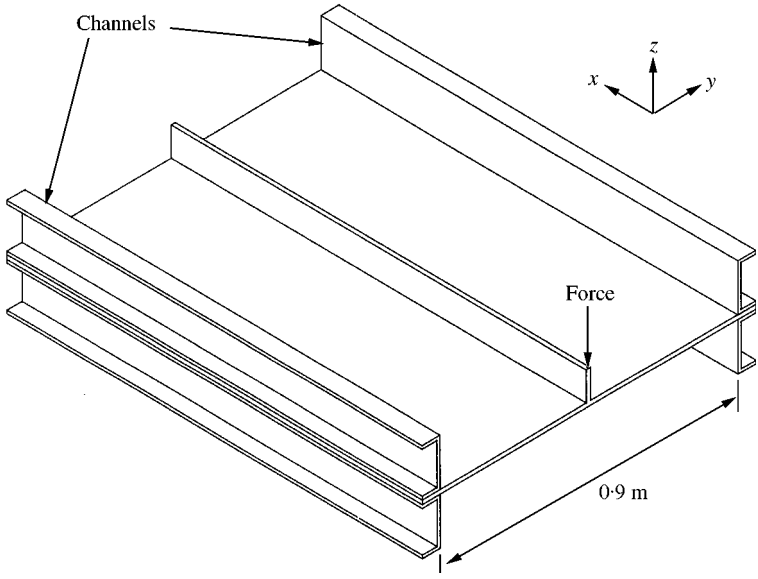

Figure 7. Sketch of the plate-stiffened beam (structure "B") with the edges clamped between $76 \times 52 \times 10$ kg/m mild steel channels [9] using large G-cramps (not shown) on each side.

where $\bar{E}_R$ is the time-averaged energy density of the receiver and η_R is its loss factor. This is related to its spatially averaged mean square velocity $\|\overline{\tilde{v}_R}|^2|$ by

$$\bar{E}_R = m''_R L_y L_e \|\overline{\tilde{v}_R}|^2|, \tag{12}$$

where m''_R is the plate mass per unit area. In section 4, laboratory measurements on two plate-stiffened beams will be presented. Because these measurements are made using piezoelectric accelerometers, it is more convenient to work with acceleration in which case the spatially averaged mean-square acceleration $\|\overline{\ddot{x}_R}|^2|$ is

$$\|\overline{\ddot{x}_R}|^2| = \frac{\omega \bar{P}_R}{\eta_R m''_R L_y L_e}. \tag{13}$$

4. MEASUREMENTS

Two slightly different perspex plate-stiffened beams similar to Figure 1 were examined in reference [1] but for brevity, only one of these structures (called structure "B" in reference [1]) will be considered here. Figure 7 shows a sketch of structure "B" in which the plate is clamped at its edges between large steel channels [9]. Jointing compound [10] was used between the plate and the channels to increase the stiffness in the clamped joint. To illustrate the versatility of the hybrid method, structure "B" is augmented with the trapezoidal plate-stiffened beam of Figure 2 (henceforth called structure "C"). To obtain the trapezoidal shape, the channels were simply rotated inward. The material properties of the perspex are shown in Table 1.

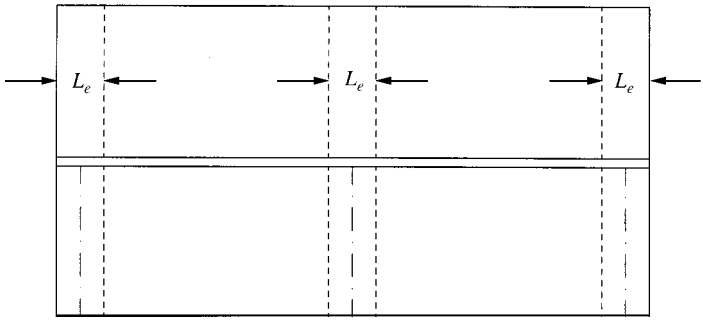

Figure 8. Plan of the plate-stiffened beam structure "B" showing the lines – · – · – along which the acceleration was measured.

4.1. MEASUREMENTS OF INPUT AND TRANSFER RESPONSE

To measure the input and transfer responses of the plate-stiffened beams, the structures were excited using an impulse hammer as described in full in reference [1].

4.2. MEASUREMENT OF THE MEAN-SQUARE RESPONSE OF THE PLATE

Since the receivers shown in Figures 3 and 6 represent the continuous plate as a set of independent receivers, the mean-square response of the plate can be estimated by measuring the plate response along lines which correspond to the receiver centrelines. Thus, measurements of the response of the plate were made at 10 randomly selected points along lines associated with three receivers as shown in Figure 8 for structure "B". For each measurement position, the beam was excited by the impulse hammer and an accelerometer measured the resulting acceleration. Ten averages were acquired for each position on the plate and the mean-square acceleration spatially averaged across all 10 positions. Table 2 shows the distances along these lines from the mid-line of the beam at which the response was measured on structure "B". Table 3 shows the position on the receivers indicated in Figure 6 at which the acceleration was measured on structure "C".

The spatially averaged mean-square acceleration determined in this manner is of course only an estimate of the true mean so confidence limits associated with a certain statistical distribution need to be determined. The number of measurement points influences the type of distribution. For sample sizes of less than 30, it is safest to assume a t-distribution since this has a wider spread than the Gaussian distribution [11]. The 90% confidence interval for the mean-square acceleration with 10 measurements is found from

$$|\|\overline{\ddot{x}_R}|^2| = \mu \pm 0{\cdot}55s, \quad s = \sigma(p-1), \tag{14}$$

where μ is the true mean and s is the sample estimate of the true standard deviation for p-samples.

TABLE 2

The distances from the mid-line of the beam at which the acceleration of the plate shown in Figure 8 was measured

Measurement number	Distance Δ_y from mid-line of beam (m)	Measurement number	Distance Δ_y from mid-line of beam (m)
1	0·039	6	0·237
2	0·103	7	0·283
3	0·143	8	0·303
4	0·176	9	0·353
5	0·209	10	0·385

TABLE 3

The distances from the mid-line of the beam at which the acceleration of the plate corresponding to the receivers nearest the middle and at the undriven end of the trapezoidal plate-stiffened beam was measured

Strip 1	Strip 13		Strip 25	
	Measurement number	Distance Δ_y from mid-line of beam (m)	Measurement number	Distance Δ_y from mid-line of beam (m)
As in Table 2	1	0·039	1	0·039
	2	0·073	2	0·063
	3	0·103	3	0·085
	4	0·123	4	0·103
	5	0·143	5	0·123
	6	0·176	6	0·143
	7	0·209	7	0·155
	8	0·237	8	0·176
	9	0·283	9	0·193
	10	0·303	10	0·209

5. DISCUSSION OF RESULTS

5.1. FINITE ELEMENT ANALYSIS OF THE BEAM ON ITS OWN

Before coupling the frequency response functions of the spine beam (as calculated by the finite element analysis) to the recceiver impedances, it is prudent to check the frequency response functions themselves. The input mobility of a free–free Euler–Bernoulli beam of length L_b driven at one end is

$$\tilde{Y}_1 = \frac{k_b}{m'_b \omega}\left(\frac{1-\tilde{\alpha}_b}{1+\tilde{\alpha}_b} - \mathrm{j}\right), \quad \tilde{\alpha}_b = \mathrm{e}^{-\mathrm{j}2\tilde{k}_b L_b}. \tag{15}$$

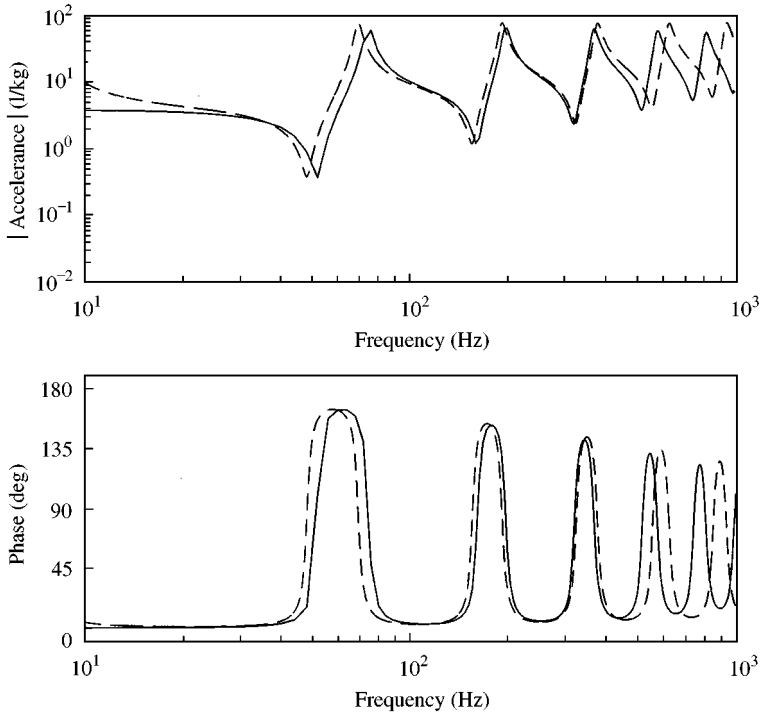

Figure 9. Predicted input accelerance of the finite beam: ——, finite element analysis; – – –, equation (14).

The transfer mobility to the undriven end of the beam is similarly

$$\tilde{Y}_{12} = \frac{k_b}{m'_b \omega}\left(\frac{-\mathrm{j}2\sqrt{\tilde{\alpha}_b}}{1+\tilde{\alpha}_b}\right). \tag{16}$$

These mobilities are inaccurate at low frequencies below $k_b L_b < 4{\cdot}6$ (15 Hz for the present structure) because below this limit the nearfield wave exceeds 1% of its amplitude at the opposite end of the beam.

Figure 9 compares the input accelerance calculated by the finite element analysis with the accelerance obtained from equation (15). The following observations are made.

(a) The resonance frequencies of the two predictions differ because the finite element model allows for shear distortion [2] which is ignored in equation (15).
(b) The low-frequency error in equation (15) is visible compared to the finite element prediction, the latter which correctly predicts a mass-like response.

These observations apply also to Figure 10 which compares the finite element transfer accelerance with the response based on equation (16). Overall, the two results indicate that the finite element analysis has yielded acceptable predictions.

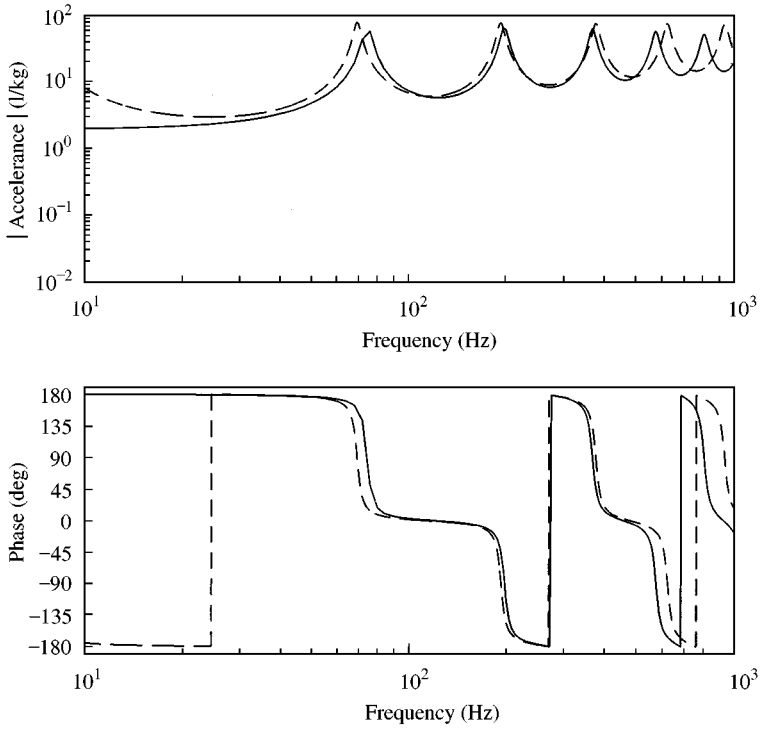

Figure 10. Predicted transfer accelerance of the finite beam: ——, finite element analysis; – – –, equation (15).

5.2. RECEIVER IMPEDANCES

Figure 11 shows the receiver impedances for the two plate-stiffened beams. Figure 11(a) shows the impedance used for all 25 receivers forming the rectangular plate. Figure 11(b) shows the 25 different impedances for the trapezoidal plate. The amplitudes are rather poorly resolved below 100 Hz due to the coarse 4 Hz frequency increment employed in the finite element analysis.

5.3. HYBRID METHOD RESULTS FOR STRUCTURE "B"

This section and the one following present the frequency response functions calculated using the hybrid method for the two plate-stiffened beams.

5.3.1. *Condition numbers for the matrix inversion and power injected into the structure*

Figure 12 shows the condition numbers for the beam mobility matrix and the coupled impedance matrix. The following observations are made:

(i) The condition numbers of the spine beam mobility matrix are generally greater than those of the coupled impedance matrix, indicating that the latter is better conditioned. This is expected because the coupled impedance matrix includes the receiver impedances on its leading diagonal.

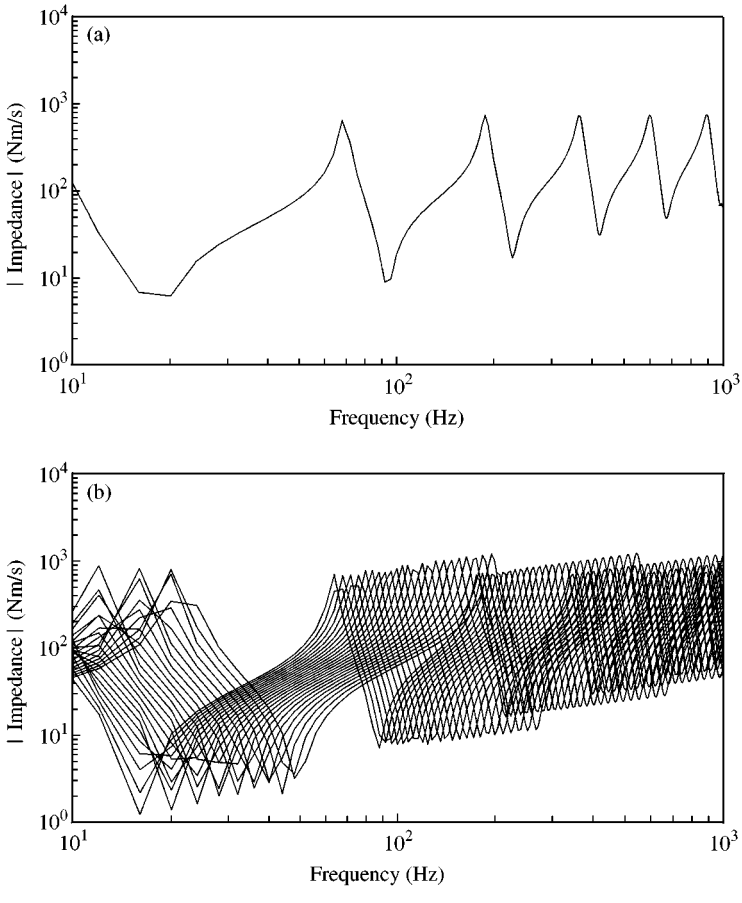

Figure 11. The receiver impedances used to model the rectangular and trapezoidal plates. (a) Rectangular plate; (b) Trapezoidal plate.

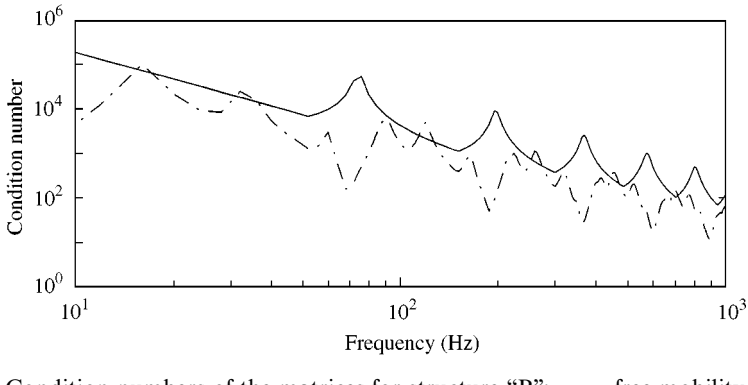

Figure 12. Condition numbers of the matrices for structure "B": ——, free mobility matrix of the spine beam; – · – · –, coupled impedance matrix of the entire structure.

(ii) The general trend is for the condition numbers to fall as the frequency increases, apart from the effects of the beam resonances such as at 75 and 200 Hz (see Figure 9). At these resonances, the magnitudes of the

input mobilities on the leading diagonal are similar to the off-diagonal transfer mobilities so the matrix condition is poorer than away from resonance.

(iii) The condition numbers do not exceed 10^6 indicating a loss of accuracy of about six decimal places and are well below the limit of equation (8).

Figure 13 shows the total power injected into the coupled structure multiplied by frequency (this makes it comparable with the imaginary part of the input

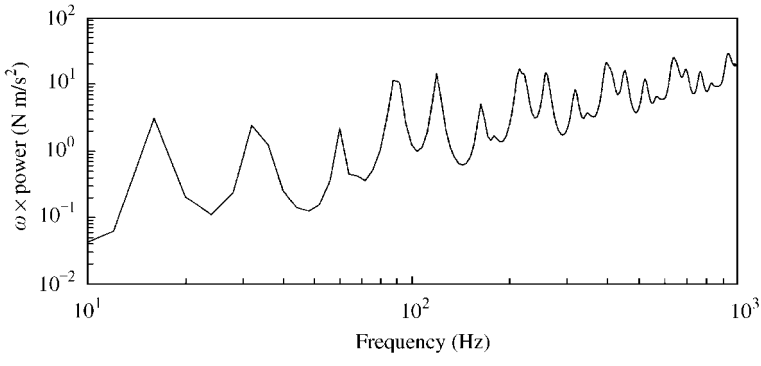

Figure 13. $\omega \times$ power injected into the plate-stiffened beam structure "B" calculated by the hybrid method.

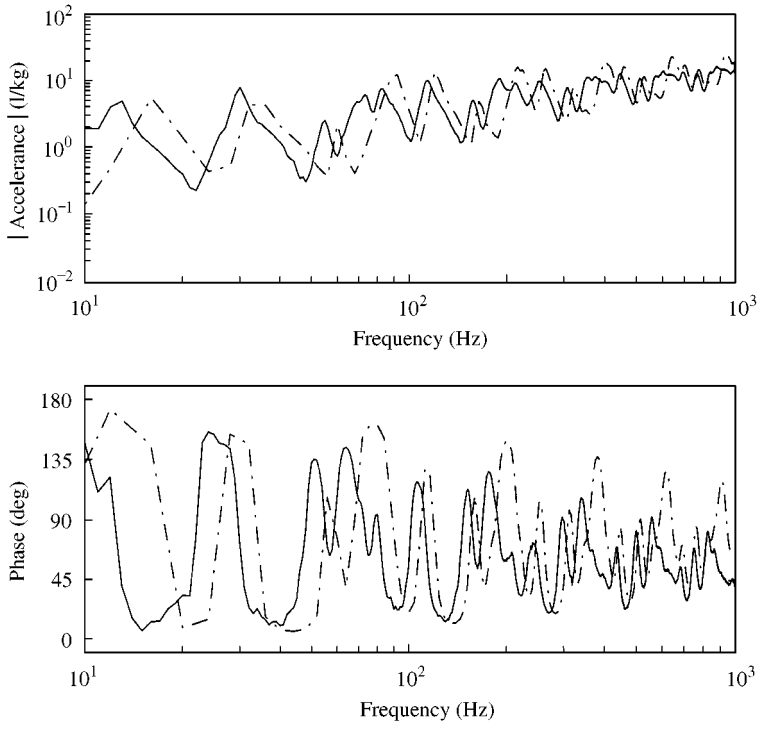

Figure 14. Input accelerance of the plate-stiffened beam structure "B": ——, measurement; – · – · –, hybrid method prediction.

accelerance) calculated by the hybrid method. All the power is positive and the data show a consistent trend. These results suggest that the hybrid method is adequately stable for the inversion of a matrix of order 27 and that the coupled responses of the structure should be admissible.

5.3.2. *Input accelerance*

Figure 14 compares the input accelerance calculated by the hybrid method with the measurement. The following observations are made.

(i) There are differences between the frequencies of the peaks and troughs of the two modulus curves and their overall levels. These are thought to be caused by the difference in the position of the beam neutral axis in the finite element analysis and the test structure

(ii) The frequency average value of the predicted phase drifts toward 90° at high frequencies.

Overall this prediction reflects the measurement except for the drift in the phase curve. This error is investigated more fully in reference [12] where it is shown that it is a function of the width of the receivers which are coupled to the beam. The phase error is believed to arise because the receivers "block" the motion of the finite elements slightly at higher frequencies, rather than modelling the continuous

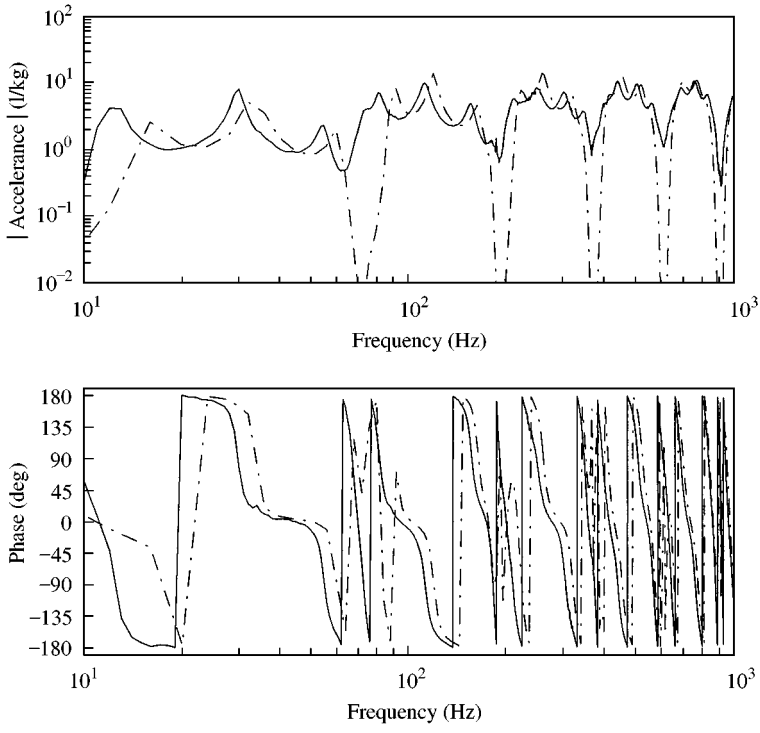

Figure 15. Transfer accelerance of the plate-stiffened beam structure "B": ——, measurement; – · – · –, hybrid method prediction.

coupling along the joint between the beam and plate. Therefore, a sufficient number of receivers is required to model the coupling properly. The present results and those in reference [12] suggest that one receiver per element (as shown in Figure 3) is the *minimum* which should be used. More receivers with a smaller width could be used but of course this would increase the order of the matrices and hence the calculation time.

5.3.3. *Transfer accelerance*

Figure 15 compares the predicted transfer response with the measurement. In general, these agree well except in a number of narrow frequency bands such

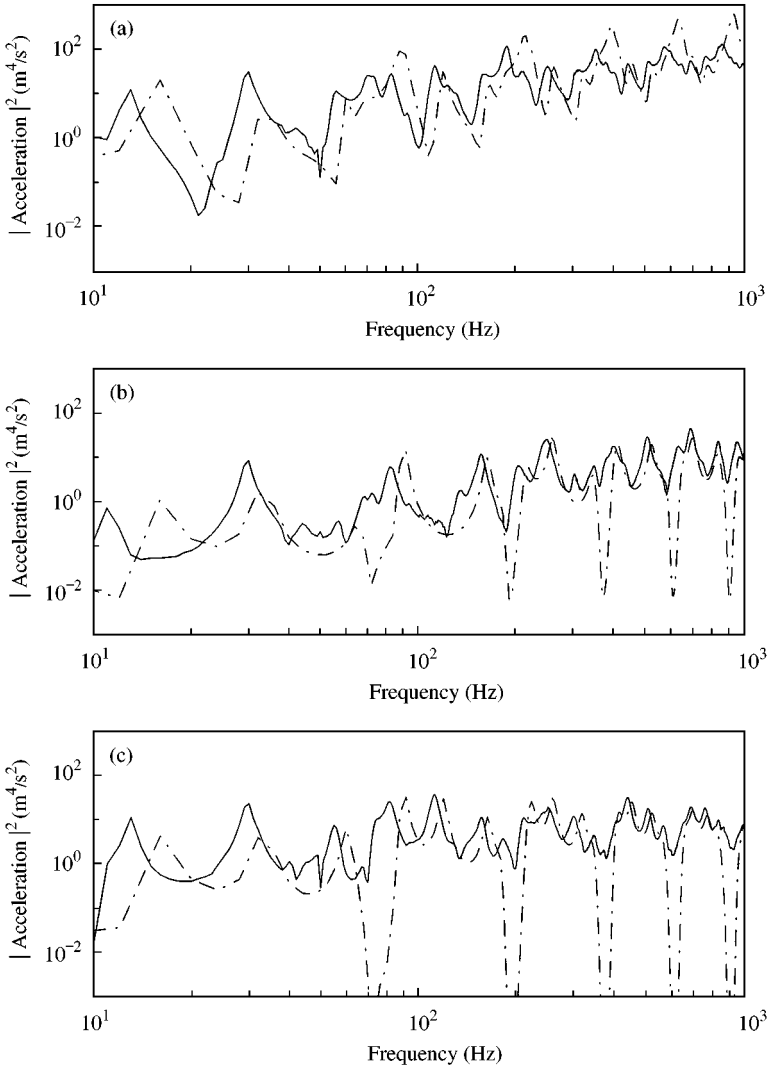

Figure 16. Mean-square acceleration for the rectangular plate of structure "B": ——, measurement; – · – · –, hybrid method prediction. (a) receiver at drive-point; (b) receiver at mid-length; (c) receiver at undriven end.

as at 200 and 400 Hz. These frequencies correspond to the peaks in the receiver impedance shown in Figure 11(a). At these frequencies the receiver is anti-resonant and therefore presents a large impedance to the entire spine, effectively blocking the transmission of waves along the beam. Thus, the rectangular plate creates a set of narrow-band vibration neutralizers as observed in references [1].

The prediction exhibits much lower vibration levels in the narrow bands of high attenuation than measured. This may be related to variations in both the width of the plate normal to the beam and the thickness of the plate noted

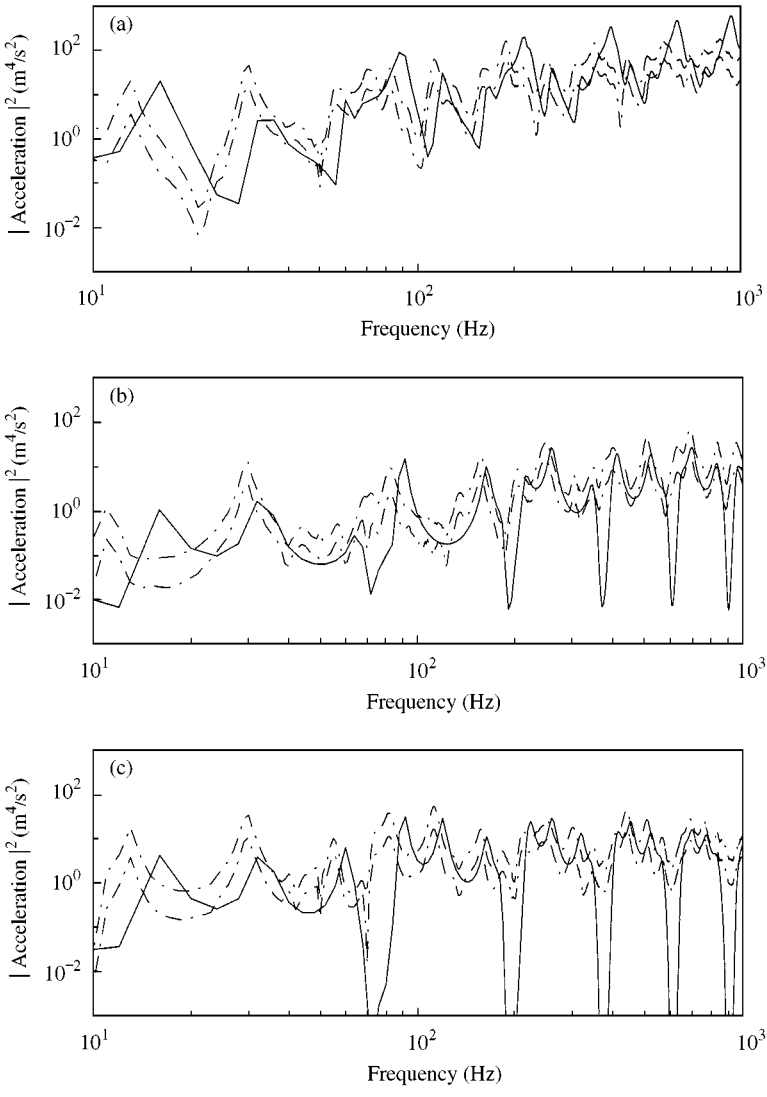

Figure 17. 90% confidence interval for the measured mean-square acceleration of the plate of structure "B": ——, predicted mean-square acceleration; – · – · –, 90% confidence limits for the measured mean. (a) receiver at drive-point; (b) receiver at mid-length; (c) receiver at undriven end.

in the structure description in reference [1]. Together, these variations are believed to prevent the plate having the precise anti-resonant impedance of equation (2) which is required to obtain maximum attenuation of the spine waves.

5.3.4. *Mean-square acceleration of the plate*

Figure 16 shows the predicted and measured mean-square acceleration for the positions on the plate shown in Figure 8. The following observations are made.

(i) The measurement taken along the line nearest the drive-point is in reasonable agreement with the prediction but shows the same frequency shift seen in the input accelerance of Figure 14.
(ii) The results at the mid- and full-length positions are in excellent agreement except below 100 Hz and in the narrow bands of high attenuation. The former error is expected to be due to the compliance of the jointing compound, while the latter error is believed to be due to the variation in plate width and thickness as mentioned above.

Figure 17 shows the 90% confidence interval for the measured mean. With the exception of the low-frequency region and within the narrow bands of high

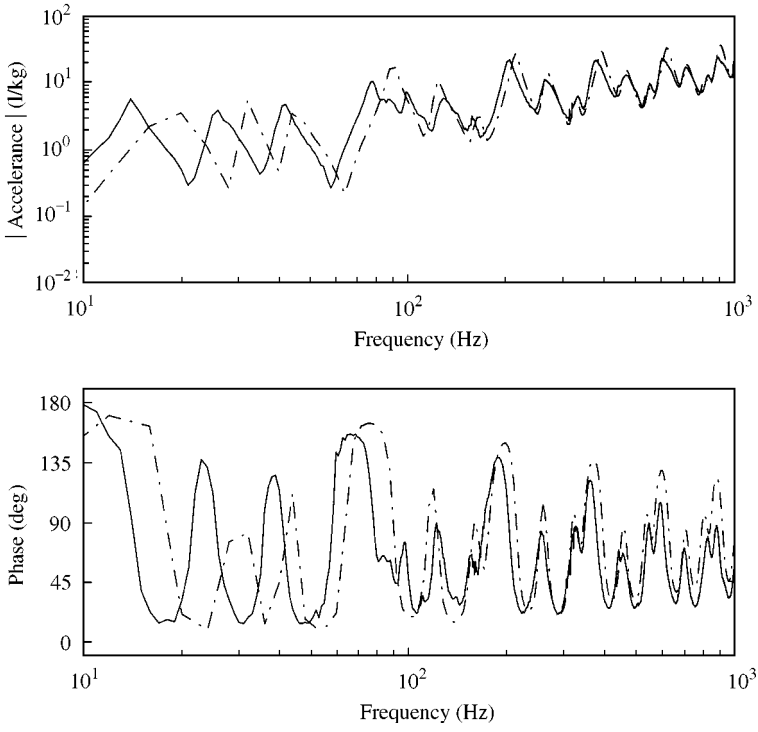

Figure 18. Input accelerance of the trapezoidal plate-stiffened beam structure "C": ——, measurement; – · – · –, hybrid method prediction.

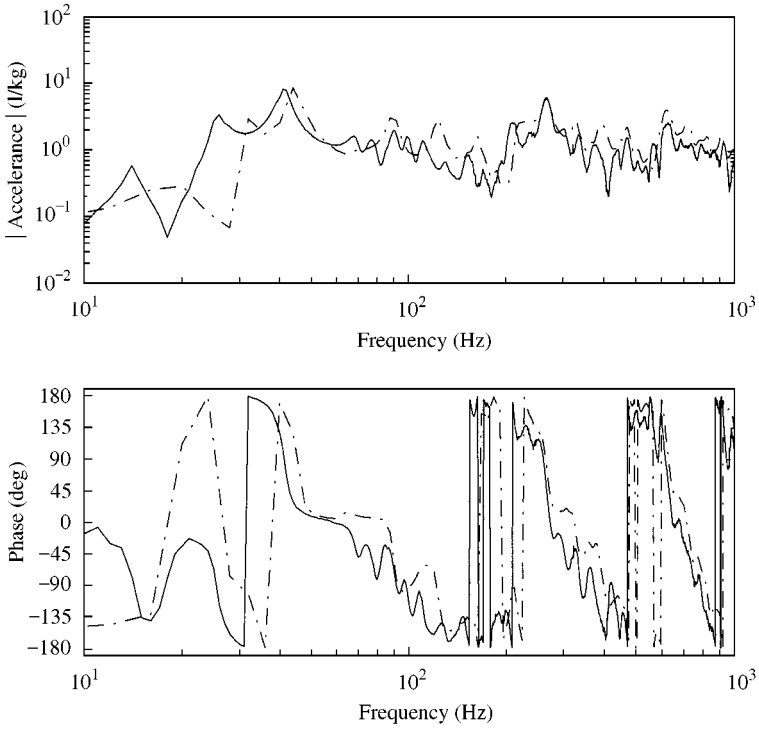

Figure 19. Transfer accelerance of the trapezoidal plate stiffened beam structure "C": ——, measurement; –·–·–, hybrid method prediction.

attenuation, the confidence interval generally encompasses the prediction which is therefore considered satisfactory.

5.4. HYBRID METHOD RESULTS FOR STRUCTURE "C"

5.4.1. *Input and transfer accelerance*

Figure 18 compares the predicted and measured input accelerances. Below 100 Hz, the peaks and troughs differ, probably because of the finite stiffness of the jointing compound used between the plate and the channels. Above 100 Hz the two curves are in excellent agreement.

Figure 19 presents the transfer accelerance and this agrees well with the measurement. In comparison with the transfer accelerance for the beam on its own shown in Figure 10, Figure 19 shows that the response at the end of the beam has been strongly reduced across the whole frequency range rather than in just narrow-frequency bands seen in Figure 15 (the vertical scale of all these figures is identical). The trapezoidal plate therefore acts as a *wideband* vibration neutraliser. Moreover, the method of modelling the plate as a set of independent plate strips reveals that, despite its trapezoidal shape, the plate remains locally reacting.

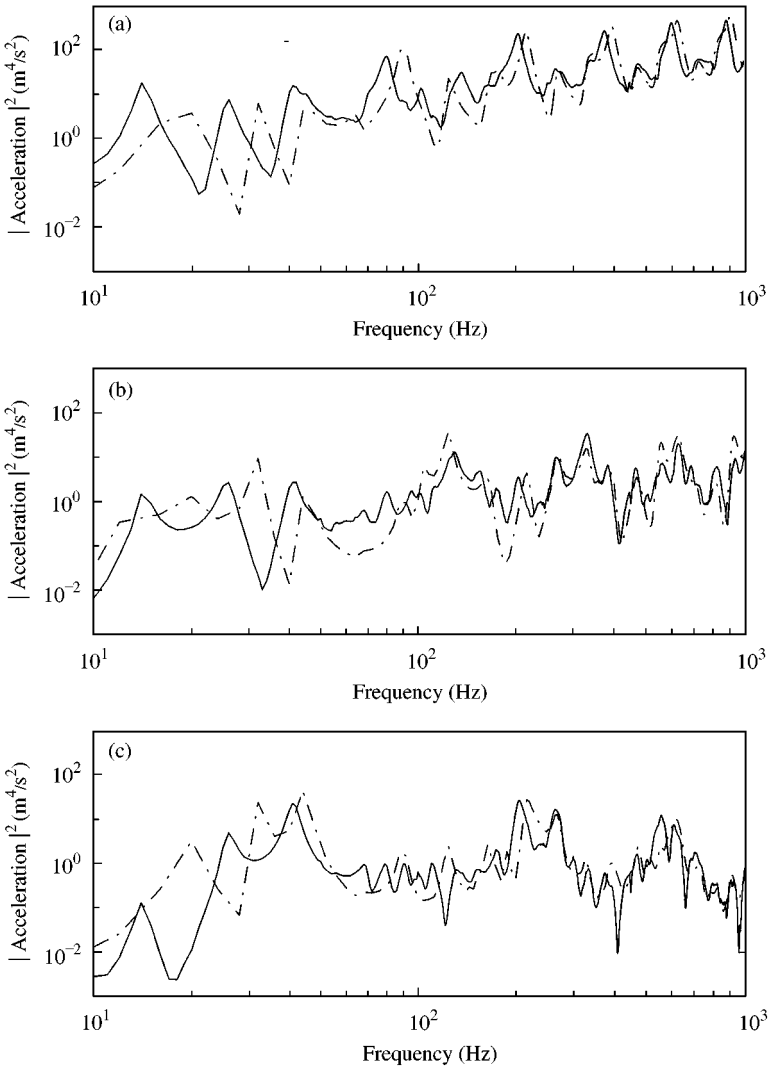

Figure 20. Mean-square acceleration for the plate of the trapezoidal plate-stiffened beam structure "C": ——, measurement; – · – · –, hybrid method prediction.

5.4.2. *Mean-square acceleration of the plate*

Figure 20 compares the predicted and measured mean-square acceleration of the three receivers shown in Figure 6. All three predictions are in good agreement with the measurements except at low frequencies due to the finite stiffness of the jointing compound. Figure 21 shows the 90% confidence interval for the measured mean which supports the predicted values.

6. CONCLUDING REMARKS

A hybrid method has been used to analyze the response of a plate-stiffened beam which consists of a single directly driven stiff beam (the spine) connected to a large

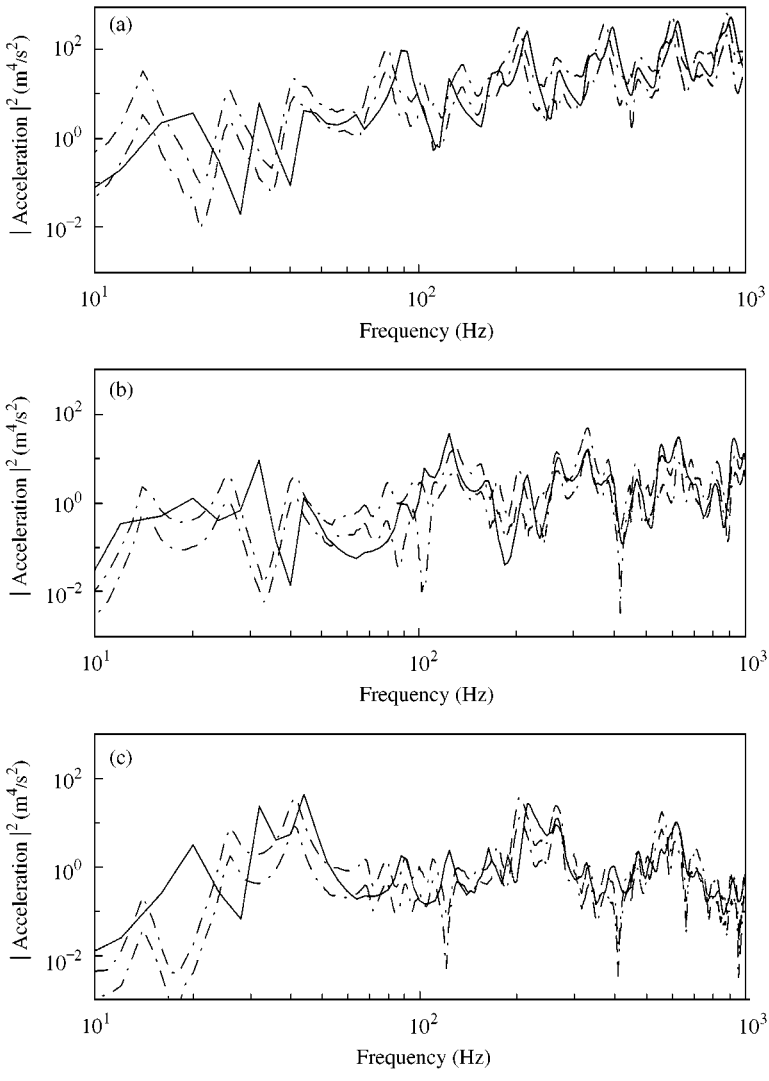

Figure 21. 90% confidence interval for the measured mean-square acceleration of the plate of the trapezoidal plate-stiffened beam structure "C": ——, predicted mean-square acceleration; – · – · –, 90% confidence limits for the measured mean.

flexible plate. The plate has been idealized as a set of narrow parallel-sided strips of plate (the receivers). The response of the spine separate from the receivers has been modelled finite element analysis. The response of the receivers separate from the spine has been modelled using analytical impedances. The two separate responses have been coupled together using a standard sub-structuring procedure. It has been shown that the following parameters must be defined in order to apply the hybrid method.

(i) The size of the element used to construct the finite element mesh of the spine must be sufficiently small such that the spine is modelled accurately.

(ii) To simulate the continuous coupling at the joint between the beam and plate, a sufficient number of receivers is required. It is suggested that the width of the receivers should be no greater than the elemental length.

(iii) The condition numbers for the matrix inversion undertaken during the sub-structuring procedure must be small enough that the calculations can be considered acceptable.

The hybrid method has been used to calculate the response of two different plate-stiffened beams. In both cases, predictions of input and transfer response on the spine beam have compared well with measurements. Additionally, the method has allowed estimation of the mean-square acceleration of the receiver plate which has also compared favourably with measurements. The predicted mean-square response of the plate could be used to predict sound radiation.

REFERENCES

1. R. M. Grice and R. J. Pinnington 1999 *Journal of Sound and Vibration* **230**, 825–849. A method for the vibration analysis of built-up structures, Part I: introduction and analytical analysis of the plate-stiffened beam.
2. L. Cremer, M. Heckl and E. E. Ungar 1988 *Structure-borne Sound*. Berlin. Springer-Verlag. second edition.
3. U. Carlsson 1993 *Ph.D. Thesis, Department of Vehicle Engineering Royal Institute of Technology, Stockholm, Sweden.* Mechanical mobility: a tool for the analysis of vibrations in mechanical structures.
4. S. D. Conte and C. De Boor 1981 *Elementary Numerical Analysis — An Algorithmic Approach.* New York: MacGraw-Hill, third edition.
5. J. J. Dongarra, J. R. Bunch, C. B. Moler and G. W. Stewart 1979 *LINPACK User's Guide.* Philadelphia, PA: SIAM.
6. M. Petyt 1990 *Introduction to Finite Element Vibration Analysis.* Cambridge, MA: Cambridge University Press.
7. *ANSYS Theory Manual* Swanson Analysis Systems Inc., Houston, USA.
8. *MATLAB Reference Guide* 1992 The Mathworks, Inc.
9. British Standard 4: Part 1: 1993 *Structural Steel Sections.* British Standards Institute, London.
10. *BOSS Green Pipe Jointing Compound* BSS (UK) Ltd., Leicester, England.
11. C. Chatfield 1993 *Statistics for Technology*. New York: Chapman & Hall, third edition.
12. R. M. Grice 1998 *Ph.D. Thesis, Southampton University*. Vibration analysis of built-up structures by combining finite element analysis and analytical impedances.

APPENDIX A: LIST OF SYMBOLS

f	Circular frequency (Hz)
j	$\sqrt{-1}$
k	wavenumber (m^{-1})
m'_b	mass per unit length (kg/m)
m''_p	mass per unit area of a plate (kg/m^2)
p	number of samples from a population (−)
n	number of bits used to store a floating point number in a computer
r	unit round-off error in storing a decimal number in binary form

s	sample estimate of standard deviation
v	velocity (m/s)
$\ddot{x}$	acceleration (m/s^2)
x, y, z	co-ordinates
D	beam stiffness (N m^2); plate stiffness (N m)
$\bar{E}$	time-averaged energy (N m)
L	length (m)
$\bar{P}$	time-averaged power (N m/s)
$\mathbf{A}$	square matrix
$\mathbf{F}$	force vector (N)
Y	structural mobility (m/s N)
Z	structural impedance (N s/m)
Z'	structural impedance per unit length (N s/m^2)
$\tilde{\alpha}, \tilde{\beta}$	travelling wave attenuation coefficients (−)
η	structural loss factor (−)
σ	standard deviation
μ	mean value
ω	radiation frequency (rad/s)